

Empowering Human-Robot Interaction Using sEMG Sensor: Hybrid Deep Learning Model for Accurate Hand Gesture Recognition

Muhammad Hamza Zafar^a, Even Falkenberg Langås^a, Filippo Sanfilippo^{a,b}

^a*Department of Engineering Sciences University of Agder Grimstad Norway*

^b*Department of Software Engineering Kaunas University of Technology Kaunas Lithuania*

Abstract

In this paper, a novel approach using a Henry Gas Solubility-based Stacked Convolutional Neural Network (HGS-SCNN) for hand gesture recognition using surface electromyography (sEMG) sensors is proposed. The stacked architecture of the CNN model helps to capture both low-level and high-level features, enabling effective representation learning. To begin, we generated a dataset comprising 600 samples of hand gestures. Next, we applied the Discrete Wavelet Transform (DWT) technique to extract features from the filtered sEMG signal. This step allowed us to capture both spatial and frequency information, enhancing the discriminative power of the extracted features. Extensive experiments are conducted to evaluate the performance of the proposed HGS-SCNN model. In addition, the obtained results are compared with state-of-the-art techniques, namely AOA-SCNN, GWO-SCNN, and WOA-SCNN. The comparative analysis demonstrates that the HGS-SCNN outperforms these existing methods, achieving an impressive accuracy of 99.3%. The experimental results validate the effectiveness of our proposed approach in accurately detecting hand gestures. The combination of DWT-based feature extraction and the HGS-SCNN model offers robust and reliable hand gesture recognition, thereby opening new possibilities for intuitive human-machine interaction and applications requiring gesture-based control.

Keywords: Surface EMG, Human-Robot Interaction, Deep Learning, Discrete Wavelet Transform

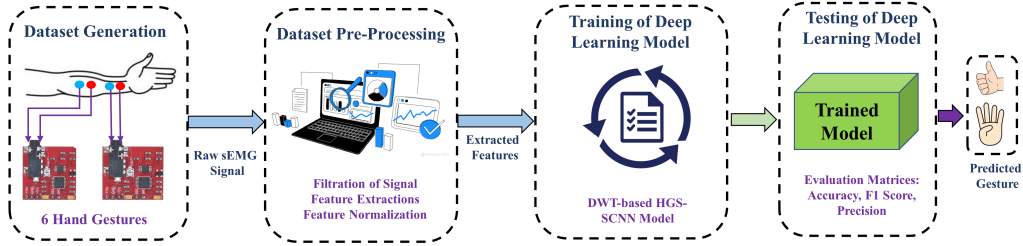


Figure 1: Proposed Hybrid DL-based Hand Gesture Detection using sEMG

10 **1. Introduction**

11 Human-robot interaction (HRI) holds significant importance in advancing in-
 12 telligent robotic systems, playing a crucial role in enabling seamless collaboration
 13 and enhancing user experience across diverse domains like healthcare, manufac-
 14 turing, and assistive technologies [1]. An essential component of effective HRI
 15 is accurate hand gesture recognition, allowing users to interact with robots natu-
 16 rally and intuitively by conveying commands, instructions, or intentions through
 17 hand movements [2]. Traditionally, vision-based techniques, involving cameras
 18 or depth sensors, have been the go-to approach for hand gesture recognition, al-
 19 though they face challenges related to lighting conditions, occlusions, variations
 20 in hand shapes, and applicability constraints in certain environments [3]. Also
 21 research is carried out on Leap motion controller based hand gesture detection in
 22 recent years [4].

23 To overcome these limitations and enhance the robustness and adaptability
 24 of hand gesture recognition in HRI, the potential of surface electromyography
 25 (sEMG) sensors is being explored. sEMG sensors are capable of detecting and
 26 recording electrical signals generated by muscle activation during hand move-
 27 ments [5]. These signals provide valuable insights into the underlying muscle ac-
 28 tivities, enabling the interpretation of intended hand gestures. Leveraging sEMG
 29 sensors for efficient hand gesture classification has led to the proposal of vari-
 30 ous machine learning (ML) and deep learning-based techniques, which will be
 31 comprehensively discussed in this literature review.

32 Machine learning has emerged as a promising solution in various fields to ad-
 33 dress and solve diverse challenges[6], [7],[8],[9]. The categorization of sEMG sig-
 34 nals using ML approaches necessitates feature extraction, i.e., time-domain [10]
 35 or frequency-domain features [11], and time-frequency domain characteristics [10].
 36 In [12], the classification of eight hand motions using the root mean square (RMS)

37 as a feature in a linear Support Vector Machine (SVM) was performed, which
38 made it possible to operate a robotic arm of 4 DoF. Altimemy et al. [13] used
39 Linear Discriminant Analysis and SVM to classify 12 hand motions for amputees
40 and 15 hand movements for those with intact limbs. In [14], Waris et al. classified
41 gesture data obtained over the course of seven days using both surface-extracted
42 EMG signals and intramuscular EMG signals, demonstrating that the performance
43 of the Artificial Neural Network (ANN) classifier has improved over time in com-
44 parison to the traditional k-nearest neighbors (KNN) and SVM classifiers.

45 Fourier inherent band functions (FIBFs) were created by dividing the sEMG
46 signals, and statistical features were then extracted for SVM and KNN classi-
47 fier [15]. By employing a jump motion device to capture the depth information,
48 which increases the relabeling of gestures in the training phase, hand gesture de-
49 tection may be improved. In [16], hand movements based on sEMG signals were
50 classified using energy-based characteristics and a fine KNN. The requirement for
51 manual feature set creation, which is a laborious operation and may not be suffi-
52 ciently precise, is a major drawback of ML systems. The difficulty in choosing
53 the best classifier for the specified characteristics is another problem.

54 Although ML algorithms have shown some promise for the categorization of
55 sEMG signals, deep learning (DL) approaches have gained popularity in recent
56 publications. It is because they tend to perform better and instantly pick up on
57 the key aspects [17]. As a result, the exoskeletons' control system may be greatly
58 enhanced by using DL approaches for the sEMG-based categorization.

59 In [18], Atzori et al. used a deep CNN architecture with two convolutional lay-
60 ers to carry out the sEMG classification job over the NinaPro DB1, DB2, and DB3
61 datasets. Compared to the KNN, SVM, Random Forests, and latent dirichlet allo-
62 cation (LDA) [19] ML classifiers currently in use, the authors have demonstrated
63 a performance gain of 2-5%. Geng et al. [20] established that instantaneous visu-
64 als include patterns that are distinguishable between trials and comparable among
65 samples of a single trial. In order to do this, they treated each sample of dimen-
66 sion 1×10 as an instantaneous picture and sent it into the CNN model as an input.
67 Metaheuristic algorithms with deep learning models have gained alot of attention
68 in recent years [21, 22, 23, 24, 25, 26].

69 A neural network variant that can handle sequential and temporal input is the
70 recurrent neural network (RNN). Koch et al. employed a ConvLSTM cascaded us-
71 ing the LSTM architecture in [27] to classify hand gesture sequences. To identify
72 the high density (HD) and sparse sEMG signals, a stacked RNN with two stage
73 networks was implemented in [28]. An attention-based CNN-RNN architecture
74 that is capable of classifying the sEMG pictures was created by Hu et al. [29]. Us-

75 ing waveform-based classification, an LSTM model and a deep back-propagation
76 (BP) LSTM were contrasted in [30].

77 *1.1. Contributions:*

78 Traditional ML and deep learning approaches for surface electromyography
79 (sEMG) signal classification in the context of hand gesture recognition, often re-
80 quire manual feature extraction, which is a laborious and time-consuming process.
81 Additionally, selecting the most appropriate classifier for the specific characteris-
82 tics of sEMG signals can be challenging. Furthermore, traditional ML and DL
83 classifiers may struggle to accurately classify sEMG signals due to their inability
84 to capture intricate patterns, inefficient tuning of hyperparameters, and exploit the
85 hierarchical representations within the data. These limitations hinder the accu-
86 racy, automation, and performance of sEMG signal classification for hand gesture
87 recognition tasks.

88 This work seeks to address the following key challenges:

- 89 • Reliance on manual feature extraction, which is laborious, time-consuming,
90 and sub-optimal. The use of automated DWT-based feature extraction over-
91 comes this.
- 92 • Inability to handle intricate spatial and temporal patterns in sEMG signals,
93 due to the use of traditional ML classifiers like SVM, KNN, ANN.
- 94 • Lack of robustness to real-world variations in hand shapes, sizes, gesture
95 dynamics etc. The large heterogeneous dataset and deep learning approach
96 aim to improve generalization.
- 97 • Difficulty in tuning hyperparameters and finding optimal network architec-
98 tures.
- 99 • Many related works only focus on limited vocabulary or hand-crafted ges-
100 tures lacking natural variability. This work uses a diversity of unrestrained
101 hand gestures.
- 102 • Reliance on visual or depth cameras, which are sensitive to environmental
103 conditions.
- 104 • Limited accuracy and reliability compared to vision-based techniques.

105 To overcome the above-mentioned problems, this work proposed a discrete
106 wavelet transform (DWT) for automatic feature extractions using sEMG onset
107 detection through moving average. After that hybrid DL model is proposed for
108 the efficient classification of hand gestures. The proposed flow of the work is
109 shown in Fig. 1. The contributions of this work are as follows:

- 110 • **Dataset Generation:** Creation of a comprehensive dataset of 600 samples,
111 providing a valuable resource for hand gesture detection research.
- 112 • **Feature Extraction with DWT:** Effective utilization of the DWT for extract-
113 ing discriminative features from hand gesture data, improving the accuracy
114 of the detection system.
- 115 • **HGS-SCNN Model:** Introduction of the novel Henry Gas Solubility-based
116 Stacked CNN (HGS-SCNN) model, demonstrating its superior performance
117 in hand gesture detection compared to alternative techniques.
- 118 • **Comparative Analysis:** Comprehensive evaluation and comparison with AOA-
119 SCNN, GWO-SCNN, and WOA-SCNN, showcasing the enhanced effec-
120 tiveness of the HGS-SCNN approach in hand gesture detection.
- 121 • **Accuracy:** Proposed DWT-based HGS-SCNN model achieves 99.3% accu-
122 racy in hand gesture detection using only 2 channels of sEMG sensors.

123 The organization of the paper is structured into various sections. Section II
124 presents a novel approach that utilizes the DWT for automated feature extraction
125 and a henry gas solubility algorithm based stacked CNN model for classification.
126 Section III explains the acquisition and preparation of the sEMG dataset used for
127 evaluation, including any preprocessing steps. Section IV presents the experimen-
128 tal results of applying the proposed technique to the dataset, discussing the per-
129 formance metrics and comparing them to previous approaches. Finally, Section V
130 summarizes the findings, highlights the contributions of the proposed technique,
131 and discusses potential avenues for future research in the field of sEMG signal
132 classification for hand gesture recognition.

133 **2. Proposed Technique:**

134 *2.1. Henry Gas Solubility Algorithm (HGS):*

135 J.W. Henry initially presented Henry’s law in 1800. In general, the most so-
136 lute that can dissolve in a given amount of solvent at a given pressure or temper-
137 ature is referred to as the solubility [31]. Consequently, HGS was motivated by

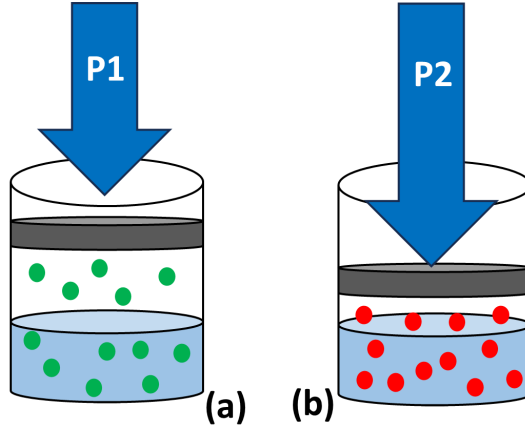


Figure 2: Working of Henry Gass Optimization (a) Movement of particles when P1 pressure is applied (b) Movement of particles when P2 pressure is applied

138 Henry's law's conduct. Henry's law may be used to calculate the solubility of low-
 139 solubility gases in liquids. Additionally, the two parameters that impact solubility
 140 are temperature and pressure. At high temperatures, solids become more soluble,
 141 whilst gases become less soluble. With respect to pressure, gas solubility rises as
 142 pressure does. As seen in Fig. 2, the subject of this algorithm is the solubility of
 143 gases.

144 In this section, the mathematical model of Henry Gas Solubility algorithm
 145 (HGS) is presented [32].

146 2.1.1. Initialization

147 The particles are randomly initialized based on the following equation:

$$X_i(t + 1) = X_{\min} + r \times (X_{\max} - X_{\min}) \quad (1)$$

148 where $X(i)$ represents the location of the i th particles among a population N , r is
 149 a number chosen at random between 0 and 1, X_{\min} and X_{\max} are the problem's
 150 upper and lower limits, and t is the number of iterations. The Eq. 2-4 serves as
 151 the start value for no. of particles i , values of Henry's constant of type j ($H_j(t)$),
 152 partial pressure of gas i in cluster j ($P_{i,j}$), and E/R constant of type j (C_i).

$$h_j = p_1 \times r \quad (2)$$

$$P_{i,j} = p_2 \times r \quad (3)$$

$$C_j = p_3 \times r \quad (4)$$

155 where p_1 , p_2 , and p_3 are defined as constants with values equal to 5×10^{-2} , 100,
 156 and 1×10^{-2} , respectively and r is the random number between 0 and 1.

157 2.1.2. Clustering:

158 The particles are separated into equal clusters, each of which is associated with
 159 a different kind of gas. Because each cluster is made up of gases that are identical
 160 to one another, they all have the same value for Henry's constant (H_j).

161 2.1.3. Evaluation:

162 The particle that achieves the greatest equilibrium state among other molecules
 163 of the same kind is determined for each cluster j . The best particle throughout the
 164 whole swarm is then determined by ranking the particles in order of performance.

165 2.1.4. Henry Coefficient Updation:

166 The solubility is updated based on the following equation:

$$S_{i,j}(t) = U \times L_j(t + 1) \times P_{i,j}(t) \quad (5)$$

167 where, $S_{i,j}$ represents the solubility of gas i in cluster j , $P_{i,j}$ is the partial pressure
 168 of gas i in cluster j , and U is a constant.

169 2.1.5. Position Updation:

170 The position is updated using the following equation:

$$X_{i,j}(t+1) = X_{i,j}(t) + F \times r \times \gamma \times (X_{best,j}(t) - X_{i,j}(t)) + F \times r \times \alpha \times (S_{i,j}(t) \times X_{best}(t)) \quad (6)$$

171 In this equation, $X_{i,j}$ denotes the location of the particle i in the cluster j ,
 172 F controls the search agent's orientation and adds diversity (pm), and r and t
 173 denote the iteration time and random constant, respectively. The best particle
 174 in the swarm is $X_{textbest}$, whereas the best particle in the cluster is $X_{textbest,j}$.
 175 Additionally, $alpha$ is the impact of other particles on particle i in cluster j (equal
 176 to 1), $beta$ is a constant, and $gamma$ reflects the capacity of gas j in cluster i to
 177 interact with other gases in its cluster. In contrast to $S_{textbest}$, which represents the
 178 fitness of the best gas in the overall system, $S_{i,j}$ specifies the fitness of gas i in
 179 cluster j . The parameters $X_{textbest,j}$ and $X_{textbest}$, which denote the best particle
 180 in the cluster j and the best particle in the swarm, respectively, play a critical role
 181 in balancing the exploration and exploitation abilities.

182 *2.1.6. Local Optimum Avoidance:*

183 The number of worst agents (denoted as N_w) is determined using the following
184 equation:

$$N_w = N \times (\text{rand}(c2 - c1) + c1) \quad (7)$$

185 Here, N represents the total number of search agents, and $c1$ and $c2$ are constants
186 with values of 0.1 and 0.2, respectively.

187 *2.2. Discrete Wavelet Transform (DWT)*

188 DWT is a mathematical tool that decomposes a signal into a set of wavelet
189 coefficients at different scales [33]. A collection of wavelet functions, which are
190 the dilations and translations of a mother wavelet function, serve as the foundation
191 for the DWT. A signal $x(n)$'s DWT is given by:

$$c_{j,k} = \langle x, \psi_{j,k} \rangle = \sum_n x(n) \psi_{j,k}(n) \quad (8)$$

192 where j and k are integer values that define the scale and translation of the wavelet
193 functions, $\psi_{j,k}(n)$ and $\phi_{j,k}(n)$ are the wavelet and scaling functions at scale j and
194 translation k , and $\langle \cdot, \cdot \rangle$ denotes the inner product between two functions. The
195 mother wavelet function $\psi(n)$ and scaling function $\phi(n)$ are dilated and trans-
196 lated to produce the wavelet and scaling functions as follows:

$$\psi_{j,k}(n) = 2^{j/2} \psi(2^j n - k) \quad (9)$$

197 The wavelet coefficients $c_{j,k}$ capture the high-frequency components of the
198 signal at scale j and translation k , while the scaling coefficients $d_{j,k}$ capture the
199 low-frequency components of the signal at scale j and translation k . The DWT
200 can be computed iteratively by applying a series of high-pass and low-pass fil-
201 ters to the signal, followed by down sampling by a factor of 2. The Daubechies
202 10 (db10) wavelet is a popular wavelet used in the DWT due to its good time-
203 frequency localization and smoothness properties. The db10 wavelet is obtained
204 by applying a series of high-pass and low-pass filters to a scaling function $\phi(n)$,
205 which is a piecewise polynomial function of degree 9. The db10 wavelet has 20
206 filter coefficients, which can be computed using the following recursive equations:

$$h_0 = \frac{1 + \sqrt{3}}{4\sqrt{2}} \quad (10)$$

$$h_1 = \frac{3 + \sqrt{3}}{4\sqrt{2}} \quad (11)$$

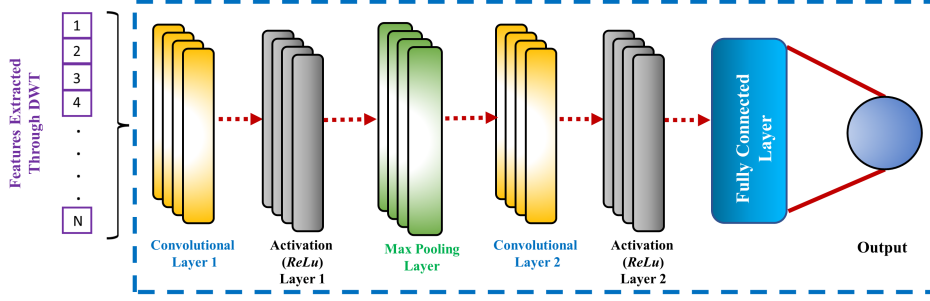


Figure 3: Proposed stacked CNN architecture with detailed layer structure

$$h_2 = \frac{3 - \sqrt{3}}{4\sqrt{2}} \quad (12)$$

$$h_3 = \frac{1 - \sqrt{3}}{4\sqrt{2}} \quad (13)$$

$$h_{4+i} = (-1)^i h_{3-i}, \quad i = 0, 1, 2, 3 \quad (14)$$

$$g_0 = h_3 \quad (15)$$

$$g_1 = -h_2 \quad (16)$$

$$g_2 = h_1 \quad (17)$$

$$g_3 = -h_0 \quad (18)$$

$$g_{4+i} = (-1)^i g_{3-i}, \quad i = 0, 1, 2, 3 \quad (19)$$

208 where h_i and g_i are the filter coefficients for the low-pass and high-pass filters,
 209 respectively. The first four coefficients, h_0 to h_3 , are the coefficients for the low-
 210 pass filter, and the remaining coefficients, h_4 to h_9 and g_4 to g_9 , are the coefficients
 211 for the high-pass filter. The remaining filter coefficients are obtained by applying
 212 a symmetry condition to the first four coefficients for both the low-pass and high-
 213 pass filters.

214 In this study, we specifically opted for the Daubechies 10 (db10) wavelet as our
215 primary mother wavelet function for conducting the Discrete Wavelet Transform
216 (DWT). The choice of db10 wavelet was grounded in its advantageous properties
217 that render it particularly suitable for our intended analysis. Firstly, db10 exhibits
218 remarkable time-frequency localization, effectively capturing transient features
219 and local patterns within the surface electromyography (sEMG) signals. This
220 precision in localization is pivotal for an accurate representation of the signal's
221 dynamics. Moreover, db10 stands out for its smoothness, a characteristic that cir-
222 cumvents the issue of abrupt discontinuities that may manifest with other wavelet
223 functions. This attribute significantly contributes to the stability of the feature
224 extraction process, ensuring a reliable and consistent analysis of the signals. An-
225 other notable quality of db10 is its possession of 10 vanishing moments, an aspect
226 critical for effectively representing complex signals by suppressing higher-order
227 polynomial behaviours. Furthermore, the db10 wavelet encompasses a set of 20
228 filter coefficients, computed through recursive relationships as defined in the rel-
229 evant literature. This distinctive feature equips the db10 wavelet with an optimal
230 filter length, enhancing its efficacy in signal processing and analysis. The care-
231 ful consideration of these properties collectively informed our decision to employ
232 the db10 wavelet as a fundamental tool for the wavelet-based analysis of sEMG
233 signals in this study.

234 Regarding the determination of decomposition levels for the Discrete Wavelet
235 Transform (DWT), a deliberate and empirical approach was taken, resulting in the
236 application of a 4-level decomposition to the surface electromyography (sEMG)
237 signals. This decision was reached through thorough experimentation involving
238 various levels, ranging from 2 to 6, with the aim of finding the most effective
239 and suitable depth for our analysis. After comprehensive testing, it became ev-
240 ident that a 4-level decomposition struck an optimal balance between frequency
241 resolution and feature dimensionality for the hand gestures under examination.
242 Lower decomposition levels were found to lack the necessary frequency resolu-
243 tion, potentially leading to an inadequate representation of signal nuances. On
244 the other hand, higher decomposition levels presented a challenge by introduc-
245 ing excessive feature dimensions without a proportional gain in informative sig-
246 nal characteristics. The 4-level decomposition was a judicious choice, offering a
247 well-rounded solution by providing localized frequency information across dis-
248 cernible sub-bands. This localization was vital for ensuring robust and effective
249 feature extraction specifically tailored to the nuances of hand gestures. The sub-
250 band distribution achieved through this decomposition proved to be particularly
251 conducive to the accurate and meaningful extraction of features from the sEMG

252 signals associated with the hand gestures being studied. Therefore, the rationale
 253 behind selecting the Daubechies 10 (db10) wavelet function and implementing a
 254 4-level DWT decomposition was grounded in achieving an optimal trade-off be-
 255 tween frequency resolution and feature dimensionality, ultimately enhancing the
 256 efficacy of the feature extraction process crucial for analyzing hand gestures in this
 257 research. These carefully considered design choices shed light on the thoughtfully
 258 constructed DWT-based feature extraction methodology utilized in this study.

259 2.3. CNN:

260 Convolutional Neural Networks (CNNs) are a class of deep learning models
 261 that have proven to be highly effective in many applications [34]. CNNs are par-
 262 ticularly well-suited for tasks involving spatial and temporal data, such as images,
 263 videos, and time-series data. CNN network uses convolutional layers to automat-
 264 ically learn hierarchical representations of the input data, which are then fed into
 265 fully connected layers for classification or regression. The detailed structure of
 266 stacked CNN is shown in Fig. 3.

267 A one-dimensional CNN is a variant of the standard CNN architecture that
 268 is designed for processing one-dimensional input data, such as time-series data or
 269 sequences of feature vectors [35]. In a 1D CNN, the input data is convolved with a
 270 set of filters, each of which slides over the input in a single dimension. The output
 271 of each filter is then passed through ReLU activation, before being downsampled
 272 using max pooling or average pooling.

273 The mathematical equations for a 1D CNN can be expressed as follows. Given
 274 an input signal $\mathbf{x} \in \mathbb{R}^{T \times C}$ and a filter $\mathbf{W}_k \in \mathbb{R}^{F \times C}$, where T is the length of the
 275 signal, C is the number of channels, and F is the filter size.

276 The convolution of the k -th filter with the input signal is computed by sliding
 277 the filter over the input channels and summing the element-wise product at each
 278 position, including a bias term b_k :

$$(W_k * x)[t] = \sum_{i=1}^C \sum_{j=0}^{F-1} w_{ki,j} \cdot x_{t+j,i} + b_k, \quad t = 1, 2, \dots, T - F + 1, \quad (20)$$

279 where $w_{ki,j}$ is the element at the i -th row and j -th column of the filter \mathbf{W}_k , $x_{t+j,i}$
 280 is the element in the i -th channel at position $t + j$ in the input signal, and b_k is the
 281 bias term for the k -th filter.

282 Apply the activation function $f(\cdot)$ to each element of the convolution result:

Table 1: Range of Hyperparameters of CNN

Parameter	Range
No. of Filters	$[2^0-2^9]$
Filter Size in Each Layer	$[1-7]$
Activation Functions	LeakyReLu, ReLu, Tanh
Learning Rate	$[10^{-5}-10^{-1}]$
Dropout Rate	$[0-0.7]$

$$z_k[t] = f((W_k * x)[t]), \quad t = 1, 2, \dots, T - F + 1 \quad (21)$$

283 The activation function introduces nonlinearity into the model. The result of the
 284 convolution and activation for the k -th filter forms a feature map \mathbf{z}_k :

$$z_k = [f((W_k * x)[1]), f((W_k * x)[2]), \dots, f((W_k * x)[T - F + 1])] \quad (22)$$

285 The feature map has a length of $(T - F + 1)$. Repeat the above steps for each
 286 filter k to obtain the complete set of feature maps $\mathbf{z}_1, \mathbf{z}_2, \dots, \mathbf{z}_K$.

$$\mathbf{z}_k = [f((W_k * x)[1]), f((W_k * x)[2]), \dots, f((W_k * x)[T - F + 1])] \quad (23)$$

287 for $k = 1, 2, \dots, K$.

288 One of the main benefits of using 1D CNNs is their ability to learn meaningful
 289 features. 1D CNNs can also capture local dependencies in the data, allowing for
 290 the detection of patterns that may not be visible at the global level. Moreover,
 291 1D CNNs can handle variable-length time series data and are robust to noise and
 292 missing values. Therefore, 1D CNNs offer a powerful and flexible approach to
 293 time series analysis that can yield state-of-the-art results in a wide range of appli-
 294 cations.

295 2.4. Hyperparameters of SCNN

296 Hyperparameters are vital components that significantly influence the perfor-
 297 mance and optimization of a stacked CNN for classification tasks. They dictate
 298 the architecture and behavior of the network, and proper selection and optimiza-
 299 tion are crucial for enhancing accuracy, convergence speed, and generalization
 300 capability. The range of hyperparameters of SCNN is shown in Table 1.

301 2.4.1. *Number and Size of Filters*

302 The number and size of filters determine the receptive field of the network.
303 While a larger number of filters can capture more diverse features, it also increases
304 computational complexity. Striking a balance between the number and size of
305 filters is important to extract relevant features efficiently.

306 2.4.2. *Kernel Size*

307 The kernel size defines the size of the convolutional window moving across the
308 input. A smaller kernel size can capture local details, while a larger kernel size
309 can capture more global patterns. Selecting an appropriate kernel size depends on
310 the characteristics of the input data and the complexity of the classification task.

311 2.4.3. *Stride and Padding*

312 The stride determines the step size of the convolutional window during the
313 convolution operation. Larger stride values reduce the spatial dimensions of the
314 output feature maps, resulting in faster processing but potentially losing fine-
315 grained details. Padding can be used to preserve spatial dimensions by adding
316 zeros around the input. Proper stride and padding selection help maintain relevant
317 information while controlling computational requirements.

318 2.4.4. *Pooling*

319 Pooling layers reduce the spatial dimensions of the feature maps, aiding in
320 translation invariance and reducing computation. Pooling can be performed using
321 operations like max pooling or average pooling. The choice of pooling size affects
322 the amount of downsampling and the retention of important features.

323 2.4.5. *Learning Rate*

324 The learning rate determines the step size during the optimization process.
325 A high learning rate may lead to overshooting and failure to converge, while a
326 low learning rate can slow down the convergence or get stuck in local optima.
327 Tuning the learning rate is essential to ensure efficient convergence and accurate
328 classification.

329 2.4.6. *Regularization*

330 Regularization techniques such as dropout and weight decay are crucial for
331 preventing overfitting, especially when dealing with limited training data. The
332 choice of regularization strength can significantly affect the model's generaliza-
333 tion ability.

334 *2.5. Importance and Difficulty of Optimization*

335 Optimizing the hyperparameters of a CNN is a critical aspect of designing
336 an effective neural network for a specific task, such as image classification. Hy-
337 perparameters are configurations that dictate the architecture, behavior, and train-
338 ing process of the neural network, distinct from the model’s learnable parameters
339 (weights and biases). Properly chosen hyperparameters can significantly influ-
340 ence the network’s performance, convergence speed, generalization ability, and
341 resource efficiency.

342 *2.5.1. Effect on Model Performance:*

343 The hyperparameters, such as the number of filters, filter sizes, learning rates,
344 and activation functions, directly affect the model’s ability to learn intricate pat-
345 terns and features from the input data. For instance, an optimal learning rate can
346 ensure faster convergence and better accuracy, while an unsuitable one might lead
347 to overshooting or slow convergence.

348 *2.5.2. Generalization and Overfitting:*

349 Hyperparameters play a pivotal role in combating overfitting, a situation where
350 the model learns to memorize the training data instead of learning useful patterns.
351 Techniques like dropout rates and weight regularization are hyperparameters cru-
352 cial for improving generalization, preventing overfitting, and making the model
353 perform well on unseen data.

354 *2.5.3. Search Space and Optimization Difficulty:*

355 The space of possible hyperparameters is vast, and the effect of each hyper-
356 parameter is often interdependent and non-linear. This complexity makes manual
357 selection impractical. Algorithms such as grid search, random search, Bayesian
358 optimization, and evolutionary methods like genetic algorithms attempt to navi-
359 gate this expansive search space efficiently.

360 *2.5.4. Computation and Time Complexity:*

361 Optimizing hyperparameters involves training and evaluating multiple mod-
362 els, making it computationally expensive and time-consuming, especially for deep
363 neural networks. The need for substantial computational resources adds to the
364 challenge, particularly when dealing with large datasets and intricate CNN archi-
365 tectures.

Table 2: Hgs based Tuned Hyperparameters of SCNN

Parameter	Range
No. of Filters	64
Filter Size in Each Layer	3
Activation Functions	ReLU
Learning Rate	10^{-2}
Dropout Rate	0.5

366 *2.5.5. Trial and Error Experimentation:*

367 Finding the optimal set of hyperparameters usually involves a trial-and-error
 368 approach, where various combinations are tested. This iterative process can be
 369 laborious and requires a good understanding of the problem, the model, and the
 370 dataset.

371 *2.6. Henry Gass Solubility based SCNN (HGS-SCNN):*

372 As described above, the main demerit of the CNN architecture is that it in-
 373 volves a large number of hyperparameters, including the size of the filters, the
 374 number of filters, and the learning rate for the optimiser. Tuning these hyperpa-
 375 rameters can be a time-consuming and challenging process, requiring extensive
 376 trial and error experimentation.

377 To address these challenges, researchers employ various techniques like grid
 378 search [36], random search [37], Bayesian optimization, or evolutionary intelligence-
 379 based methods such as genetic algorithms (GAs) [38], particle swarm optimisa-
 380 tion (PSO) or Grey wolf optimizer (GWO). These algorithms are designed to effi-
 381 ciently search for optimal hyperparameters by exploring the hyperparameter space
 382 using heuristic techniques and mathematical optimisation methods. In this work,
 383 we employed the Henry Gas Solubility (HGS) algorithm to tune the hyperparam-
 384 eters of the CNN architecture. The proposed flow of HGS based SCNN model is
 385 shown in Fig. 4, while the tuned hyperparameters of the SCNN model are shown
 386 in Table 2.

387 *2.7. Motivation of using HGS Algorithm:*

388 The selection of the Henry Gas Solubility (HGS) algorithm for hyperparame-
 389 ter tuning in the Stacked Convolutional Neural Network (SCNN) is underpinned
 390 by the aspiration for an optimization technique that resonates with the intrinsic na-
 391 ture of the hand gesture recognition problem. The HGS algorithm, inspired by gas
 392 solubility principles, presents a nature-inspired optimization approach. Emulating

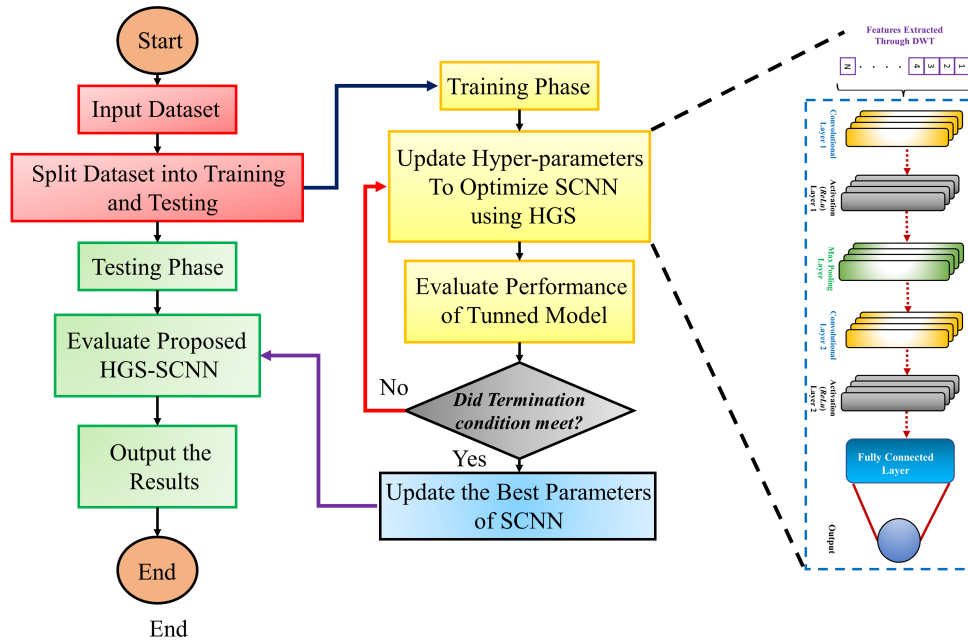


Figure 4: Hyperparameter Tuning Flow of Proposed HGS-SCNN technique

393 the behaviour of gas molecules in confined spaces, it offers a novel perspective to
 394 solving optimization problems. One of the pivotal motivations for employing this
 395 approach is its efficiency in exploring the high-dimensional hyperparameter space
 396 characteristic of SCNNs. By simulating the diffusion of gas molecules, the algo-
 397 rithm strives to efficiently navigate this space, crucial for discovering an optimal
 398 set of hyperparameters significantly impacting SCNN performance. Moreover,
 399 the gas-inspired exploration carries the potential to achieve global optimization, a
 400 desirable trait for developing a robust SCNN model with improved generalization
 401 capabilities, particularly in the domain of hand gesture recognition. This approach
 402 aligns seamlessly with the fundamental design principles of CNNs, particularly in
 403 feature extraction tasks, making it a suitable choice for optimizing SCNNs.

404 3. Dataset Collection and Processing:

405 3.1. Dataset Generation:

406 The dataset consists of surface electromyography (sEMG) signals recorded
 407 from 2 sensors interfaced with an Arduino MEGA 2560 microcontroller. Data
 408 are collected from 5 subjects performing 6 different gestures and every gesture

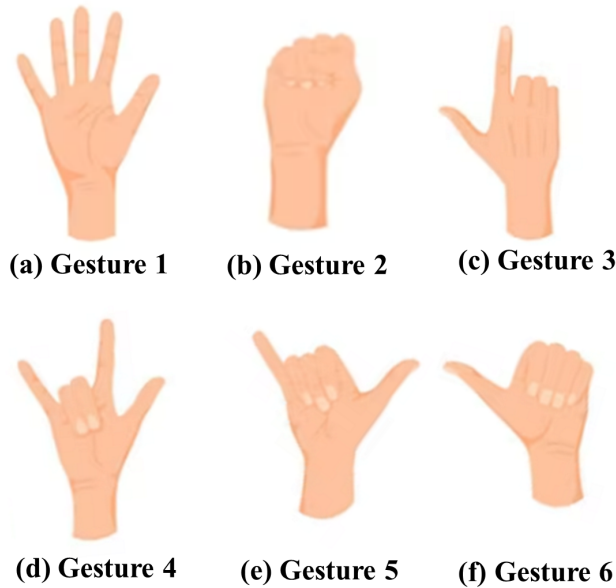


Figure 5: Hand Gestures used for Dataset Generation and Classification

409 is repeated 20 times, resulting in a comprehensive dataset for training and eval-
410 uation. The hardware setup involves connecting the Arduino MEGA 2560 with
411 MATLAB Simulink 2022a. This integration allows for real-time data acquisi-
412 tion and communication with the microcontroller board. Two sEMG sensors are
413 connected to the Arduino MEGA, providing simultaneous recording of muscle
414 activation signals from multiple hand muscles. The six hand gestures used for
415 dataset generation are shown in Fig. 5.

416 The sEMG sensors used in this study are non-invasive electrodes that detect
417 electrical signals generated by muscle contractions. These sensors are carefully
418 placed on specific hand muscles to capture the corresponding muscle activation
419 patterns during hand gestures. Subjects were instructed to position the sensors
420 according to standardized electrode placement guidelines. A well-defined ges-
421 ture protocol was employed to ensure consistency across data collection sessions.
422 Each hand gesture consisted of an action phase and a rest phase, both lasting 2
423 seconds. During the action phase, subjects were instructed to perform the target
424 hand gesture, while the rest phase involved relaxation with no intentional mus-
425 cle activity. This protocol aimed to capture the distinct sEMG patterns associated
426 with each gesture.

Table 3: Specifications for the hand gesture dataset generation

variable	Value
No. of Subject	5
No. of Gestures	6
No. of Channels	2
No. of Repetitions	20
Sampling Frequency (Hz)	1000
Activity Duration (s)	2
Rest Time (s)	2

427 Data collection sessions were conducted with 5 subjects, who were briefed
 428 about the experimental procedure and provided informed consent. Each subject
 429 performed the 6 hand gestures, with 20 repetitions per gesture. The order of ges-
 430 tures was randomized to minimize any potential order effects. Subjects were given
 431 adequate rest intervals between repetitions and gestures to minimize muscle fa-
 432 tigue. During the data collection process, the sEMG signals were continuously
 433 recorded from the sensors at a sampling rate of 1000 Hz. This high sampling
 434 rate ensured capturing fine-grained details of the muscle activation signals. The
 435 acquired signals were transmitted in real-time from the Arduino MEGA to MAT-
 436 LAB Simulink for further processing and storage. The dataset generated from the
 437 data collection process comprised a total of 120 instances for each subject (20 rep-
 438 etitions x 6 gestures). Considering the 5 subjects, the final dataset consisted of 600
 439 instances. This sufficiently large dataset facilitates robust training and evaluation
 440 of hand gesture recognition models. The specifications of the dataset generation
 441 are shown in Table 3.

442 3.2. Filtering:

443 Filtering is a crucial preprocessing step in enhancing the quality and relia-
 444 bility of electromyography (EMG) signals. In this study, a bandpass filter with
 445 a frequency range of 20 Hz to 300 Hz was employed to selectively pass sig-
 446 nals within the desired frequency band while attenuating frequencies outside this
 447 range. This specific frequency range was chosen based on its biological rele-
 448 vance to muscle activation patterns and the need to remove low-frequency noise
 449 and high-frequency interference [39]. By implementing the bandpass filter, un-
 450 wanted noise, such as baseline drift and power line interference, was effectively
 451 eliminated, allowing for a clearer representation of the underlying muscle activity.

452 The implementation of the bandpass filter involved employing suitable digital
453 signal processing techniques. The filter's performance was evaluated by assessing
454 its frequency response, magnitude response, and phase response. This evaluation
455 ensured that the bandpass filter effectively attenuated out-of-band noise while pre-
456 serving the relevant frequency components within the 20 Hz to 300 Hz range.

457 3.3. Feature Extractions:

458 The analysis of sEMG sensor data of hand gestures involves a multi-step pro-
459 cess to extract meaningful information and features. The initial step in this flow
460 is to calculate the moving average of the signal. This is accomplished by apply-
461 ing a sliding window technique, where the average value of the signal within a
462 specific window size is computed. The moving average helps to reduce noise and
463 smooth out the signal, enhancing the visibility of underlying patterns and features
464 related to hand gestures. By utilizing this technique, the overall signal quality is
465 improved, enabling subsequent analysis steps to be more effective.

466 Following the calculation of the moving average, the next crucial step is EMG
467 onset detection. EMG onset refers to the initiation of muscle activity associated
468 with the hand gesture. Detecting the precise onset of EMG activity is vital for
469 accurately capturing the relevant data during the hand gesture performance. Var-
470 ious techniques can be employed for EMG onset detection, such as amplitude
471 threshold-based methods, slope-based methods, or ML algorithms. These ap-
472 proaches analyze the characteristics of the moving average signal and identify
473 the point at which the EMG activity exceeds a certain threshold or exhibits a sig-
474 nificant change, indicating the start of the hand gesture.

475 After identifying the EMG onset, a sample window of 300 milliseconds is se-
476 lected from the original signal. This window represents a segment of the signal
477 that encapsulates the duration of the hand gesture. In this segment, the DWT is
478 performed to extract valuable features. DWT reveals both the time and frequency
479 domain information simultaneously. By applying DWT to the sample window,
480 the signal is analyzed at various scales or levels of resolution, providing a multi-
481 resolution representation of the hand gesture. Features such as amplitude, fre-
482 quency content, and energy distribution across different frequency sub-bands can
483 be extracted from the DWT coefficients. These features capture important charac-
484 teristics of the hand gesture, enabling further analysis, classification or recognition
485 tasks. The comparison of extracted features using DWT for different gestures is
486 shown in Fig. 6.

487 The Discrete Wavelet Transform (DWT) plays a crucial role in the process of
488 extracting distinct and discernible features from surface electromyography (sEMG)

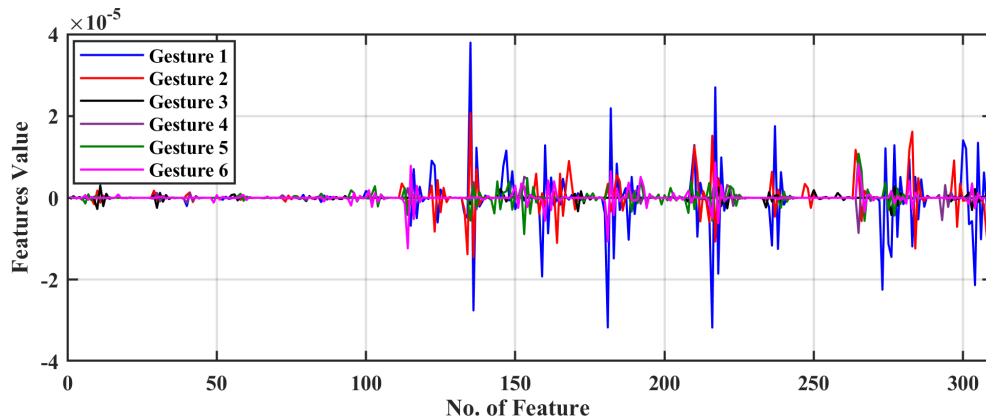


Figure 6: Extracted features through DWT from Channel 1

489 signals for hand gesture recognition. By employing wavelet functions, the DWT
 490 breaks down the signal into various frequency sub-bands at different scales, re-
 491 vealing both time and frequency domain information in a simultaneous manner.
 492 The lower frequency bands provide insight into the global contour and overall
 493 trends present within the signal, while the higher frequency bands capture tran-
 494 sient spikes and local patterns. Through wavelet coefficients, the distribution of
 495 energy across these sub-bands is made evident, showcasing how different ges-
 496 tures manifest distinct coefficient distributions. For instance, a pinch gesture may
 497 exhibit a higher concentration of high-frequency coefficients compared to a grip
 498 gesture. The advantage of wavelets lies in their ability to be localized in time,
 499 enabling the capture of transient muscle activation spikes. The multi-resolution
 500 view that DWT offers accentuates the nuances tied to gesture dynamics, revealing
 501 patterns that might not be visible when examining just the raw signal. Therefore,
 502 the DWT not only surfaces hidden patterns but also accentuates subtleties, provid-
 503 ing an augmented feature space when compared to using solely raw sEMG data
 504 or basic statistical measures. In summary, DWT decomposes the signal in a man-
 505 ner that uncovers unique spatio-temporal and spectral characteristics of muscle
 506 activity associated with each gesture, facilitating a more robust feature extraction
 507 and discrimination compared to utilizing only the original sEMG recordings. Feel
 508 free to let me know if this elucidation adequately conveys how DWT contributes
 509 to distinctive feature extraction.

510 *3.4. Dataset Pre-Processing:*

511 Normalizing the data is an essential step in data preprocessing, as it helps
512 to improve the performance of many ML algorithms. One of the most common
513 normalization techniques is the min-max scaling technique. In this technique, the
514 values of a feature are scaled to a range between 0 and 1. The min-max scaling
515 technique is given by the following equation:

$$X_{norm} = \frac{X - X_{min}}{X_{max} - X_{min}} \quad (24)$$

516 where X is current sample, X_{min} and X_{max} are the min. and max. values of the
517 sample, and X_{norm} is the normalized sample value.

518 *3.5. Evaluation Matrices*

519 Evaluation matrices are commonly used to assess the performance of clas-
520 sification models, including those used for hand gesture recognition. Here, we
521 present four widely used evaluation matrices: Accuracy, Precision, Specificity,
522 and F1 score. These matrices depend upon the True positive (TP), True Negative
523 (TN), False Positive (FP) and False Negative (FN) of the predicted classes.

524 *3.6. Accuracy*

525 Accuracy is the ratio of the correctly predicted samples to the total number of
526 samples in the dataset;

$$Accuracy = \frac{TP + TN}{Totalnumberofsamples} \quad (25)$$

527 *3.7. Precision*

528 Precision is a metric that indicates how well the model performs in terms of
529 minimizing false positives:

$$Precision = \frac{TP}{TP + FP} \quad (26)$$

530 *3.8. Specificity*

531 Specificity is a metric that indicates how well the model performs in terms of
532 minimizing false negatives:

$$Specificity = \frac{TN}{TN + FP} \quad (27)$$

Table 4: Gesture Prediction Comparative Analysis

Technique	Accuracy	Precision	Specificity	F1 Score
HGS-SCNN	0.9944	0.9944	0.9989	0.9944
AOA-SCNN	0.9778	0.9778	0.9756	0.9778
WOA-SCNN	0.9611	0.9611	0.9622	0.9613
GWO-SCNN	0.9556	0.9556	0.9512	0.9557

533 3.9. F1 Score

534 The F1-score is calculated as:

$$F1Score = 2 \times \frac{Precision \times Recall}{Precision + Recall} \quad (28)$$

535 These evaluation matrices help in assessing the performance of hand gesture
 536 classification models and provide insights into the model’s accuracy, precision,
 537 specificity, and overall effectiveness.

538 3.10. Proposed Scheme:

539 The flow of analysis for sEMG sensor data of hand gestures involves multiple
 540 steps. First, the moving average of the signal is calculated to reduce noise and
 541 enhance the visibility of underlying patterns. Next, the EMG onset is detected
 542 to pinpoint the time window associated with the hand gesture. Subsequently, a
 543 sample window is selected, and the DWT is applied to extract informative fea-
 544 tures from the signal. This systematic approach provides a scientific framework
 545 for processing and analyzing sEMG data, facilitating the understanding and in-
 546 terpretation of hand gestures for various applications such as prosthetics, reha-
 547 bilitation, or human-computer interaction systems. After feature extraction and
 548 pre-processing, the dataset is divided into 70-30% training and testing dataset ra-
 549 tios. After that, the HGS-based SCNN model is trained on training data and tested
 550 on the testing dataset to check the performance of the proposed model. The de-
 551 tailed DWT-based HGS-SCNN scheme for hand gesture detection is elaborated
 552 in Fig. 7. Fig. 8 shows the loss and accuracy of tuned SCNN model. A detailed
 553 analysis on the results is presented in the next section.

554 4. Results and Analysis:

555 4.1. Prediction Performance

556 The evaluation of prediction performance for different techniques based on
 557 stacked CNN networks (SCNN) in classifying six distinct hand gestures is pre-

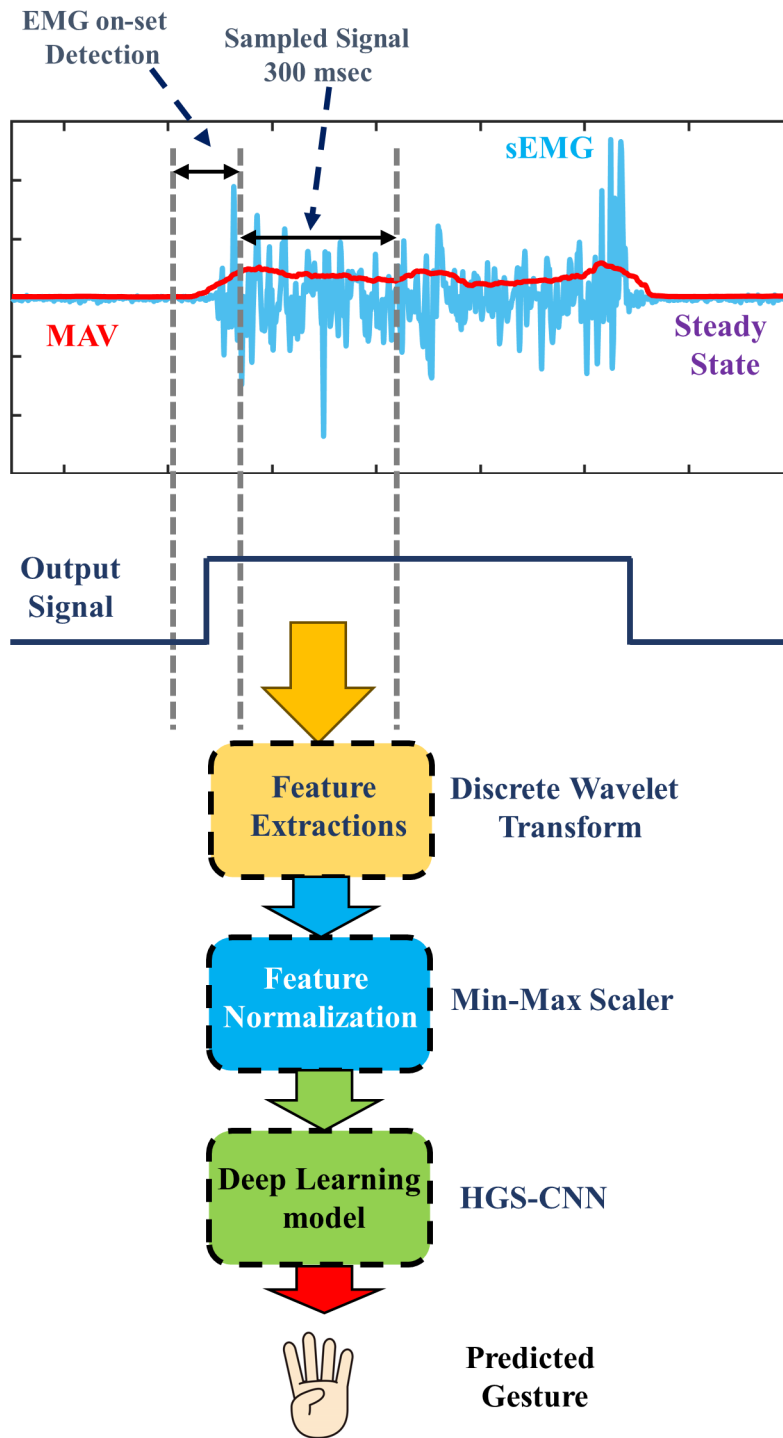


Figure 7: Proposed DWT-based HGS-CNN technique

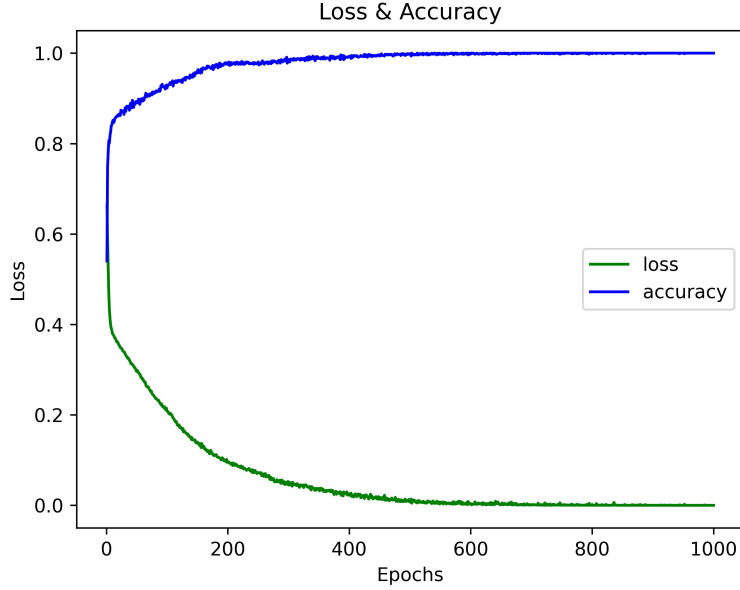


Figure 8: Loss and Accuracy curve of the HGS tuned SCNN model

558 sented in Table 4. To delve deeper into the predictive abilities of these techniques,
 559 a thorough analysis utilizing confusion matrices (as depicted in Fig. 9) and a compar-
 560 ative evaluation of key metrics (shown in Fig. 10) is conducted. A compre-
 561 hensive breakdown and analysis of these results are presented in the subsequent
 562 subsections.

563 4.1.1. Accuracy

564 Accuracy is a fundamental metric reflecting the proportion of correctly pre-
 565 dicted instances out of the total. Among the techniques analyzed, HGS-SCNN
 566 stands out with the highest accuracy of 0.9944. This implies an outstanding ability
 567 to predict hand gestures with a staggering accuracy rate of 99.44%. AOA-SCNN
 568 closely follows with an accuracy of 0.9778, indicating a slightly lower but still im-
 569 pressive accuracy rate of 97.78%. WOA-SCNN achieves an accuracy of 0.9611,
 570 demonstrating a high precision but slightly less than the previous two techniques.
 571 GWO-SCNN, while effective, exhibits the lowest accuracy among the listed tech-
 572 niques, with a value of 0.9556.

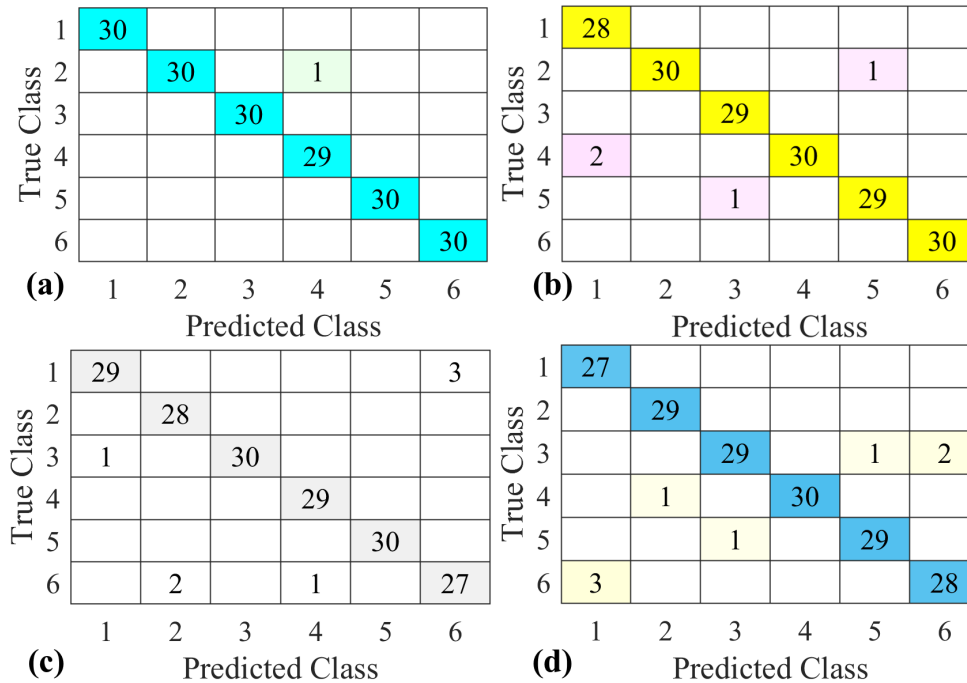


Figure 9: Confusion Matrix Comparison of (a) HGS-SCNN, (b) AOA-SCNN, (c) WOA-SCNN and (d) GWO-SCNN

573 *4.1.2. Precision*

574 Precision is a crucial measure denoting the proportion of true positive predic-
 575 tions out of all predicted positives. HGS-SCNN leads in precision with a score of
 576 0.9944, implying that 99.44% of the hand gestures predicted as positive by HGS-
 577 SCNN are indeed correct. AOA-SCNN closely follows with a precision score of
 578 0.9778, indicating a high level of precision in its predictions. WOA-SCNN and
 579 GWO-SCNN also demonstrate substantial precision scores of 0.9611 and 0.9556,
 580 respectively, signifying a high level of correctness in their positive predictions.

581 *4.1.3. Specificity*

582 Specificity measures the ability to identify non-target gestures accurately. HGS-
 583 SCNN excels in specificity, achieving the highest score of 0.9989. This suggests
 584 that HGS-SCNN identifies non-target gestures with an impressive accuracy rate of
 585 99.89%. AOA-SCNN follows with a specificity of 0.9756, indicating a high level
 586 of accuracy in identifying non-target gestures. WOA-SCNN and GWO-SCNN

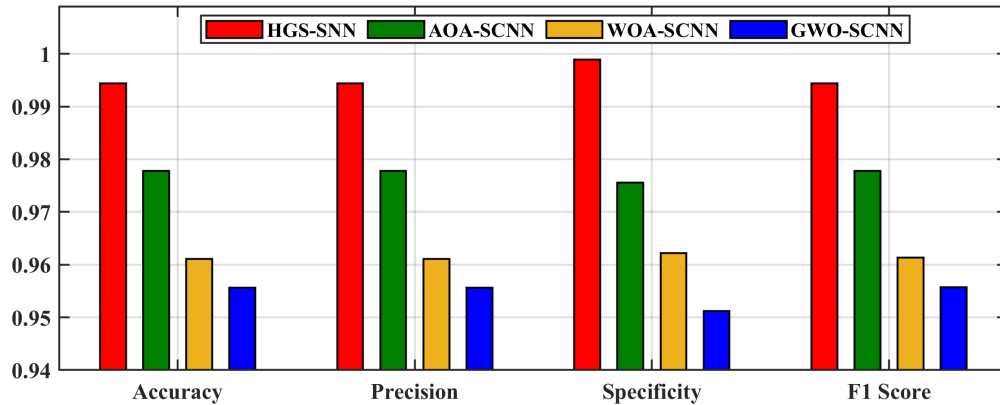


Figure 10: Bar Graph Comparison of Competing Techniques

587 also exhibit commendable specificity scores of 0.9622 and 0.9512, respectively,
 588 underscoring their ability to discern non-target gestures with substantial accuracy.

589 4.1.4. F1 Score

590 The F1 score, a balanced metric considering both precision and recall, pro-
 591 vides a comprehensive assessment of the overall predictive performance. HGS-
 592 SCNN achieves an F1 score of 0.9944, suggesting a harmonious trade-off between
 593 precision and recall and indicating a high overall performance. AOA-SCNN
 594 closely follows with an F1 score of 0.9778, representing a balanced performance
 595 in terms of precision and recall. WOA-SCNN and GWO-SCNN also present re-
 596 spectable F1 scores of 0.9613 and 0.9557, respectively. These scores emphasize
 597 the ability of these techniques to strike a balance between precision and recall,
 598 contributing to a robust overall predictive performance.

599 Based on the results presented in Table 4, HGS-SCNN stands out by showcasing
 600 superior performance compared to the other techniques. Several key aspects
 601 highlight its exceptional capabilities:

- 602 • High Accuracy: HGS-SCNN attains the highest accuracy among all the
 603 techniques, signifying its remarkable precision in predicting hand gestures.
- 604 • High Precision: HGS-SCNN achieves an impressive precision score of 0.9944,
 605 indicating an extremely low false positive rate. Consequently, the gestures
 606 predicted as positive by HGS-SCNN are highly likely to be accurate.
- 607 • High Specificity: HGS-SCNN secures the highest specificity among the

Table 5: Comparative Analysis of Hand Gesture Detection Presented in Literature

Ref.	Data-set	Technique Used	Acc.
[40]	Indian Sign Language(Pictorial static coloured images) 6	Feature Selection + NN for Classification (trained using hybrid meta-heuristic deer hunting + gwo)	0.97
[41]	Spatial Data-set (Arabic Sign Language Numerals 1-9)	Radial Basis Function	0.942
[42]	Static 9 gestures	FS(static; based on Orientation) + SVM Classification	0.9137
[43]	Six static images	HOG + SVM (multi-class)	0.92
[44]	Three static gestures (Rock, paper, scissors)	FS (static 11 points) + DNN Classification	0.98
<i>Our approach</i>	Six Hand gestures	HGS Algorithm based Stacked CNN	0.993

608 techniques, showcasing its remarkable ability to precisely identify non-
 609 target gestures. This aspect is crucial in avoiding false positives.

- 610 • High F1 Score: HGS-SCNN achieves a well-balanced F1 score of 0.9944,
 611 showcasing its adeptness in maintaining an effective trade-off between pre-
 612 cision and recall. This score signifies that HGS-SCNN excels in minimizing
 613 both false positives and false negatives.

614 4.2. Comparative Analysis

615 The Table 5 presented provides a comparative analysis of various hand gesture
 616 detection techniques found in the literature. Each technique is evaluated based on
 617 the dataset used, the specific methodology employed, and the accuracy achieved.
 618 Among the listed approaches, our proposed technique stands out as a superior
 619 solution.

620 Firstly, the proposed technique utilizes a comprehensive dataset consisting of
 621 six hand gestures. In contrast, other references in the table used datasets with spe-
 622 cific sign language gestures, spatial data, or a limited number of static images. The

623 breadth and depth of our dataset suggest a more representative and robust training
624 environment. Secondly, the proposed technique leverages a stacked convolutional
625 neural network (CNN) algorithm for hand gesture detection. CNNs have proven
626 to be highly effective in image-related tasks, thanks to their ability to identify pat-
627 terns and extract features from visual data. This choice of algorithm showcases
628 the sophistication and advanced nature of our approach. In comparison, the other
629 techniques in the table include feature selection with ANN, RBF functions, SVM
630 with feature selection, and deep neural networks (DNN). While these techniques
631 are valuable in their respective contexts, our utilization of a stacked CNN algo-
632 rithm demonstrates a more cutting-edge and potentially more accurate approach.
633 Lastly, the proposed technique achieves an outstanding accuracy of 0.993, sur-
634 passing the accuracies reported in the other references. The highest accuracy in
635 the table is 0.98, achieved by a DNN-based approach for a limited set of three
636 hand gestures. The significantly higher accuracy of our proposed technique high-
637 lights its exceptional capability in accurately classifying and recognizing hand
638 gestures. This level of accuracy is vital for real-world applications where precise
639 and reliable gesture detection is required.

640 **5. Discussion**

641 In this section, we delve into the insights and implications drawn from the pre-
642 sented results and the comparative analysis of hand gesture detection techniques.

643 *5.1. Performance Comparison and Interpretations*

644 The evaluation of prediction performance using stacked CNN networks (SCNN)
645 for hand gesture classification has showcased the outstanding performance of the
646 HGS-SCNN technique. With an accuracy of 0.9944, HGS-SCNN has demon-
647 strated a remarkable ability to accurately predict hand gestures. Such high accu-
648 racy is of paramount importance, particularly in applications like human-computer
649 interaction and robotics, where precise gesture recognition is a critical factor. The
650 high precision of HGS-SCNN (0.9944) underscores its capability to maintain an
651 extremely low false positive rate, implying that the predicted hand gestures are
652 highly likely to be correct. This characteristic is vital in applications where in-
653 accurate predictions could lead to adverse outcomes. Furthermore, HGS-SCNN
654 exhibited the highest specificity (0.9989) among the techniques analyzed, show-
655 casing its proficiency in accurately identifying non-target gestures. This aspect is
656 crucial in gesture recognition systems to avoid false positives, which can be par-
657 ticularly detrimental in applications such as medical diagnostics. The well-balanced

658 F1 score of 0.9944 achieved by HGS-SCNN emphasizes its effectiveness in main-
659 taining a trade-off between precision and recall. This is a vital characteristic for
660 achieving a high-performing model that minimizes both false positives and false
661 negatives.

662 In contrast to the HGS-SCNN model, the competitive techniques, namely
663 GWO-SCNN, WOA-SCNN, and AOA-SCNN, exhibit suboptimal performance
664 in the classification of hand gestures, yielding comparatively lower values across
665 evaluation matrices. Specifically, GWO-SCNN encounters challenges in effec-
666 tively fine-tuning the Stacked CNN (SCNN) model, resulting in a suboptimal
667 resolution with convergence being hindered in local minima during the cost re-
668 duction process. The resultant accuracy achieved by GWO-SCNN is recorded at
669 95.56%. AOA-SCNN and WOA-SCNN demonstrate relatively higher accuracy in
670 comparison to GWO-SCNN. AOA-SCNN leverages a superior exploration strat-
671 egy, enabling it to navigate away from local minima, thereby contributing to its
672 elevated accuracy. Similarly, WOA-SCNN, while exhibiting less accuracy than
673 AOA-SCNN, outperforms GWO-SCNN, showcasing a more proficient optimiza-
674 tion in the SCNN model tuning process. AOA-SCNN and WOA-SCNN attain
675 accuracy values of 97.78% and 96.11%, respectively. However, it is notewor-
676 thy that the HGS-SCNN model surpasses GWO-SCNN, WOA-SCNN, and AOA-
677 SCNN across all evaluated metrics. The efficacy of HGS-SCNN is attributed to its
678 adeptness in avoiding local minima through a judicious interplay of exploration
679 and exploitation phases. This attribute enhances the model’s capacity for accurate
680 classification of hand gestures, positioning it as a superior choice compared to
681 GWO-SCNN, WOA-SCNN, and AOA-SCNN in the studied context.

682 5.2. Comparative Analysis and Key Insights

683 The comparative analysis of various hand gesture detection techniques high-
684 lighted the strengths of the proposed HGS-SCNN approach. Our technique lever-
685 aged a comprehensive dataset encompassing six diverse hand gestures, providing
686 a more representative and robust training environment compared to other tech-
687 niques that used specific sign language gestures or a limited set of static images.

688 The adoption of a stacked convolutional neural network (CNN) algorithm
689 demonstrated the advanced nature of our approach. CNNs are known for their
690 effectiveness in image-related tasks due to their ability to identify intricate pat-
691 terns and extract features from visual data. This choice of algorithm underlines
692 our commitment to employing cutting-edge methodologies for hand gesture de-
693 tection.

694 Lastly, achieving an accuracy of 0.993 with our proposed technique surpassed
695 the accuracies reported in other references, underscoring its superior performance.
696 This high accuracy level hints at the potential practical applicability of our ap-
697 proach in various domains.

698 *5.3. Practical Implications, Challenges and Future Avenues*

699 The superior performance of HGS-SCNN in hand gesture detection carries
700 significant practical implications across multiple domains. In human-computer in-
701 teraction, our technique has the potential to significantly enhance user experience
702 by providing accurate and intuitive gesture-based control systems. In the field of
703 robotics, precise gesture recognition can enable seamless and efficient control of
704 robotic devices, contributing to advancements in automation and robotics.

705 While the proposed HGS-SCNN model shows impressive accuracy in hand
706 gesture recognition, like any technology, it's not without its limitations. One po-
707 tential challenge lies in variations in sensor conditions. Real-world scenarios may
708 involve different environments, lighting conditions, or hardware variations, which
709 could affect the performance of the model. The model might struggle to gener-
710 alize well across diverse conditions not accounted for during training. Moreover,
711 user-specific nuances can be a hurdle. People have unique ways of performing
712 hand gestures, and individual differences in anatomy, muscle structure, or even
713 the placement of the sEMG sensors can introduce variability. The model might
714 not adapt perfectly to all users, potentially leading to lower accuracy or misclas-
715 sifications for certain individuals. The effectiveness of the model could be in-
716 fluenced by the size and diversity of the dataset used for training. If the dataset
717 does not adequately represent the wide range of potential users and scenarios,
718 the model might not generalize well to unforeseen conditions. Furthermore, the
719 reliance on the Discrete Wavelet Transform (DWT) for feature extraction might
720 introduce limitations. While DWT is effective in capturing spatial and frequency
721 information, it might not be optimal for all types of hand gestures or could be sen-
722 sitive to certain signal variations. It's crucial to consider these limitations when
723 implementing the HGS-SCNN model in practical applications. Ongoing research
724 and refinement could address these challenges, making the model more robust and
725 adaptable to a broader range of conditions and user-specific nuances.

726 For future research, further exploration of deep learning architectures and op-
727 timization techniques could potentially elevate the accuracy and efficiency of hand
728 gesture detection systems. Additionally, investigating the application of hand ges-
729 ture detection in real-time and dynamic environments would provide valuable in-
730 sights for practical deployments, such as in gaming, virtual reality, and assistive

731 technologies.

732 **6. Conclusion**

733 This paper introduced a novel approach for hand gesture detection using a
734 Henry Gas Solubility-based Stacked Convolutional Neural Network (HGS-SCNN).
735 Hand gesture detection has become increasingly important in various domains,
736 and our proposed approach offers enhanced accuracy and robustness in this task.
737 The stacked architecture of the CNN model allows for effective representation
738 learning by capturing both low-level and high-level features.

739 Through the utilization of the Discrete Wavelet Transform (DWT) technique
740 for feature extraction, our approach successfully captures spatial and frequency
741 information, leading to improved discriminative power in the extracted features.
742 Extensive experiments were conducted using a dataset of 600 hand gesture sam-
743 ples, and the performance of the HGS-SCNN model was evaluated. Comparative
744 analysis with SOTA techniques demonstrates the superiority of our proposed ap-
745 proach, achieving an impressive accuracy of 99.3%.

746 The results validate the effectiveness of our approach in accurately detecting
747 hand gestures and highlight the potential of combining DWT-based feature extrac-
748 tion with the HGS-SCNN model. This combination offers reliable and robust hand
749 gesture recognition, opening up new possibilities for intuitive human-computer or
750 human-robot interaction and applications that require gesture-based control.

751 Possible future works that can be further carried out are elaborated below:

- 752 • Expanding the gesture vocabulary - The current 6 gestures, while cover-
753 ing a useful range, are still limited. Adding more complex uni-manual and
754 bimanual gestures can enhance the system's capabilities.
- 755 • Evaluating personalized models - Training user-specific models that adapt
756 to individual variations in muscle anatomy and sEMG patterns may further
757 boost accuracy.
- 758 • Exploring sensor fusion - Supplementing sEMG with inertial or depth data
759 could make the recognition more robust to ambiguities.

760 **Acknowledgment**

761 This research is supported by the Biomechatronics and Collaborative Robotics
762 research group at the Top Research Center Mechatronics (TRCM), University of
763 Agder (UiA), Norway.

764 **References**

- 765 [1] O. Mazhar, B. Navarro, S. Ramdani, R. Passama, A. Cherubini, A real-
766 time human-robot interaction framework with robust background invariant
767 hand gesture detection, *Robotics and Computer-Integrated Manufacturing*
768 60 (2019) 34–48.
- 769 [2] N. Mendes, Surface electromyography signal recognition based on deep
770 learning for human-robot interaction and collaboration, *Journal of Intelli-
771 gent & Robotic Systems* 105 (2) (2022) 42.
- 772 [3] H. Chen, M. C. Leu, Z. Yin, Real-time multi-modal human–robot collab-
773 oration using gestures and speech, *Journal of Manufacturing Science and
774 Engineering* 144 (10) (2022) 101007.
- 775 [4] H. Mohyuddin, S. K. R. Moosavi, M. H. Zafar, F. Sanfilippo, A compre-
776 hensive framework for hand gesture recognition using hybrid-metaheuristic
777 algorithms and deep learning models, *Array* (2023) 100317.
- 778 [5] S. A. Khomami, S. Shamekhi, Persian sign language recognition using imu
779 and surface emg sensors, *Measurement* 168 (2021) 108471.
- 780 [6] F. Belmajdoub, S. Abderafi, Efficient machine learning model to predict fine-
781 ness, in a vertical raw meal of morocco cement plant, *Results in Engineering*
782 17 (2023) 100833.
- 783 [7] J. Zhou, Y. Dai, M. Tao, M. Khandelwal, M. Zhao, Q. Li, Estimating the
784 mean cutting force of conical picks using random forest with salp swarm
785 algorithm, *Results in Engineering* 17 (2023) 100892.
- 786 [8] A. Nazir, A. K. Shaikh, A. S. Shah, A. Khalil, Forecasting energy consump-
787 tion demand of customers in smart grid using temporal fusion transformer
788 (tft), *Results in Engineering* 17 (2023) 100888.
- 789 [9] S. Sreelakshmi, G. Malu, E. Sherly, R. Mathew, M-net: An encoder-decoder
790 architecture for medical image analysis using ensemble learning, *Results in
791 Engineering* 17 (2023) 100927.
- 792 [10] A. Phinyomark, E. Scheme, An investigation of temporally inspired time
793 domain features for electromyographic pattern recognition, in: 2018 40th
794 Annual International Conference of the IEEE Engineering in Medicine and
795 Biology Society (EMBC), IEEE, 2018, pp. 5236–5240.

- 796 [11] A. Phinyomark, P. Phukpattaranont, C. Limsakul, Feature reduction and se-
797 lection for emg signal classification, *Expert systems with applications* 39 (8)
798 (2012) 7420–7431.
- 799 [12] P. Shenoy, K. J. Miller, B. Crawford, R. P. Rao, Online electromyographic
800 control of a robotic prosthesis, *IEEE transactions on biomedical engineering*
801 55 (3) (2008) 1128–1135.
- 802 [13] A. H. Al-Timemy, R. N. Khushaba, G. Bugmann, J. Escudero, Improving
803 the performance against force variation of emg controlled multifunctional
804 upper-limb prostheses for transradial amputees, *IEEE Transactions on Neu-
805 ral Systems and Rehabilitation Engineering* 24 (6) (2015) 650–661.
- 806 [14] A. Waris, I. K. Niazi, M. Jamil, K. Englehart, W. Jensen, E. N. Kamavuako,
807 Multiday evaluation of techniques for emg-based classification of hand mo-
808 tions, *IEEE journal of biomedical and health informatics* 23 (4) (2018)
809 1526–1534.
- 810 [15] B. Fatimah, P. Singh, A. Singhal, R. B. Pachori, Hand movement recognition
811 from semg signals using fourier decomposition method, *Biocybernetics and
812 Biomedical Engineering* 41 (2) (2021) 690–703.
- 813 [16] N. K. Karnam, A. C. Turlapaty, S. R. Dubey, B. Gokaraju, Classification of
814 semg signals of hand gestures based on energy features, *Biomedical Signal
815 Processing and Control* 70 (2021) 102948.
- 816 [17] Y. LeCun, Y. Bengio, G. Hinton, Deep learning, *nature* 521 (7553) (2015)
817 436–444.
- 818 [18] M. Atzori, M. Cognolato, H. Müller, Deep learning with convolutional neu-
819 ral networks applied to electromyography data: A resource for the classifica-
820 tion of movements for prosthetic hands, *Frontiers in neurorobotics* 10 (2016)
821 9.
- 822 [19] M. Atzori, A. Gijsberts, C. Castellini, B. Caputo, A.-G. M. Hager, S. Elsig,
823 G. Giatsidis, F. Bassetto, H. Müller, Electromyography data for non-invasive
824 naturally-controlled robotic hand prostheses, *Scientific data* 1 (1) (2014) 1–
825 13.
- 826 [20] W. Geng, Y. Du, W. Jin, W. Wei, Y. Hu, J. Li, Gesture recognition by instan-
827 taneous surface emg images, *Scientific reports* 6 (1) (2016) 36571.

- 828 [21] M. H. Zafar, M. Mansoor, M. Abou Houran, N. M. Khan, K. Khan, S. K. R.
829 Moosavi, F. Sanfilippo, Hybrid deep learning model for efficient state of
830 charge estimation of li-ion batteries in electric vehicles, *Energy* 282 (2023)
831 128317.
- 832 [22] S. K. Raza Moosavi, M. H. Zafar, S. Mirjalili, F. Sanfilippo, Improved barna-
833 cles movement optimizer (ibmo) algorithm for engineering design problems,
834 in: *International Conference on Artificial Intelligence and Soft Computing*,
835 Springer, 2023, pp. 427–438.
- 836 [23] A. Muqet, A. Israr, M. H. Zafar, M. Mansoor, N. Akhtar, A novel opti-
837 mization algorithm based pid controller design for real-time optimization of
838 cutting depth and surface roughness in finish hard turning processes, *Results*
839 *in Engineering* 18 (2023) 101142.
- 840 [24] Z. A. Kadhuim, S. Al-Janabi, Codon-mrna prediction using deep optimal
841 neurocomputing technique (dlstm-dsn-woa) and multivariate analysis, *Re-*
842 *sults in Engineering* 17 (2023) 100847.
- 843 [25] V. Balaji, S. Narendranath, et al., Optimization of wire-edm process param-
844 eters for ni–ti–hf shape memory alloy through particle swarm optimization
845 and cnn-based sem-image classification, *Results in Engineering* 18 (2023)
846 101141.
- 847 [26] J. F. Ruma, M. S. G. Adnan, A. Dewan, R. M. Rahman, Particle swarm
848 optimization based lstm networks for water level forecasting: a case study
849 on bangladesh river network, *Results in Engineering* 17 (2023) 100951.
- 850 [27] P. Koch, M. Dreier, M. Maass, H. Phan, A. Mertins, Rnn with stacked ar-
851 chitecture for semg based sequence-to-sequence hand gesture recognition,
852 in: *2020 28th European Signal Processing Conference (EUSIPCO)*, IEEE,
853 2021, pp. 1600–1604.
- 854 [28] I. Ketykó, F. Kovács, K. Z. Varga, Domain adaptation for semg-based ges-
855 ture recognition with recurrent neural networks, in: *2019 International Joint*
856 *Conference on Neural Networks (IJCNN)*, IEEE, 2019, pp. 1–7.
- 857 [29] Y. Hu, Y. Wong, W. Wei, Y. Du, M. Kankanhalli, W. Geng, A novel attention-
858 based hybrid cnn-rnn architecture for semg-based gesture recognition, *PLoS*
859 *one* 13 (10) (2018) e0206049.

- 860 [30] Y. Wang, Q. Wu, N. Dey, S. Fong, A. S. Ashour, Deep back propagation–
861 long short-term memory network based upper-limb semg signal classifica-
862 tion for automated rehabilitation, *Biocybernetics and Biomedical Engineer-*
863 *ing* 40 (3) (2020) 987–1001.
- 864 [31] V. Mohebbi, A. Naderifar, R. Behbahani, M. Moshfeghian, Determination
865 of henry’s law constant of light hydrocarbon gases at low temperatures, *The*
866 *Journal of Chemical Thermodynamics* 51 (2012) 8–11.
- 867 [32] F. A. Hashim, E. H. Houssein, M. S. Mabrouk, W. Al-Atabany, S. Mirjalili,
868 Henry gas solubility optimization: A novel physics-based algorithm, *Future*
869 *Generation Computer Systems* 101 (2019) 646–667.
- 870 [33] G. Othman, D. Q. Zeebaree, The applications of discrete wavelet transform
871 in image processing: A review, *Journal of Soft Computing and Data Mining*
872 1 (2) (2020) 31–43.
- 873 [34] C. Tian, Y. Xu, Z. Li, W. Zuo, L. Fei, H. Liu, Attention-guided cnn for image
874 denoising, *Neural Networks* 124 (2020) 117–129.
- 875 [35] A. Kanwal, M. F. Lau, S. P. Ng, K. Y. Sim, S. Chandrasekaran, Bicudnnlstm-
876 1dcnn—a hybrid deep learning-based predictive model for stock price pre-
877 diction, *Expert Systems with Applications* 202 (2022) 117123.
- 878 [36] F. J. Pontes, G. Amorim, P. P. Balestrassi, A. Paiva, J. R. Ferreira, Design of
879 experiments and focused grid search for neural network parameter optimiza-
880 tion, *Neurocomputing* 186 (2016) 22–34.
- 881 [37] J. Bergstra, Y. Bengio, Random search for hyper-parameter optimization.,
882 *Journal of machine learning research* 13 (2) (2012).
- 883 [38] M. Ilbeigi, M. Ghomeishi, A. Dehghanbanadaki, Prediction and optimiza-
884 tion of energy consumption in an office building using artificial neural net-
885 work and a genetic algorithm, *Sustainable Cities and Society* 61 (2020)
886 102325.
- 887 [39] S. Ma, B. Lv, C. Lin, X. Sheng, X. Zhu, Emg signal filtering based on
888 variational mode decomposition and sub-band thresholding, *IEEE journal*
889 *of biomedical and health informatics* 25 (1) (2020) 47–58.

- 890 [40] M. Kowdiki, A. Khaparde, Automatic hand gesture recognition us-
891 ing hybrid meta-heuristic-based feature selection and classification with
892 dynamic time warping, *Computer Science Review* 39 (2021) 100320.
893 doi:<https://doi.org/10.1016/j.cosrev.2020.100320>.
- 894 [41] W. Zeng, C. Wang, Q. Wang, Hand gesture recognition using leap motion via
895 deterministic learning, *Multimedia tools and applications* 77 (2018) 28185–
896 28206.
- 897 [42] Y. Xu, Q. Wang, X. Bai, Y.-L. Chen, X. Wu, A novel feature extracting
898 method for dynamic gesture recognition based on support vector machine,
899 in: *2014 IEEE International Conference on Information and Automation*
900 *(ICIA)*, 2014, pp. 437–441. doi:[10.1109/ICInfA.2014.6932695](https://doi.org/10.1109/ICInfA.2014.6932695).
- 901 [43] K.-p. Feng, F. Yuan, Static hand gesture recognition based on hog charac-
902 ters and support vector machines, in: *2013 2nd International Symposium on*
903 *Instrumentation and Measurement, Sensor Network and Automation (IM-*
904 *SNA)*, 2013, pp. 936–938. doi:[10.1109/IMSNA.2013.6743432](https://doi.org/10.1109/IMSNA.2013.6743432).
- 905 [44] Q. Yang, W. Ding, X. Zhou, D. Zhao, S. Yan, Leap motion hand
906 gesture recognition based on deep neural network, in: *2020 Chi-*
907 *nese Control And Decision Conference (CCDC)*, 2020, pp. 2089–2093.
908 doi:[10.1109/CCDC49329.2020.9164723](https://doi.org/10.1109/CCDC49329.2020.9164723).